Journal of Physics D:
Applied Physics

PAPER

Flexible strain sensor array for accurate recognition of handwriting features and trajectory

To cite this article: Lin Cheng *et al* 2025 *J. Phys. D: Appl. Phys.* **58** 235504

IOP Publishing Journal of Physics D: Applied Physics
J. Phys. D: Appl. Phys. **58** (2025) 235504 (8pp) https://doi.org/10.1088/1361-6463/add747

Flexible strain sensor array for accurate recognition of handwriting features and trajectory

Lin Cheng[1,5], Ziyi Pei[1,5], Zheyang Yu[1], Diqing Ruan[1,2], Shujia Song[3], Huaping Wu[4] and Aiping Liu[1,*]

[1] Zhejiang Key Laboratory of Quantum State Control and Optical Field Manipulation, Department of Physics, Zhejiang Sci-Tech University, Hangzhou 310018, People's Republic of China
[2] Zhejiang Key Laboratory of Digital Precision Measurement Technology Research, Zhejiang Institute of Quality Sciences, Hangzhou 310018, People's Republic of China
[3] School of Mechanical Engineering, Zhejiang Sci-Tech University, Hangzhou 310018, People's Republic of China
[4] Key Laboratory of Special Purpose Equipment and Advanced Processing Technology, Ministry of Education and Zhejiang Province, College of Mechanical Engineering, Zhejiang University of Technology, Hangzhou 310023, People's Republic of China

E-mail: liuaiping1979@gmail.com

Received 1 February 2025, revised 6 May 2025
Accepted for publication 12 May 2025
Published 22 May 2025

Abstract

Handwriting recognition systems face critical challenges in achieving concurrent high sensitivity, rapid response, and real-time multi-dimensional signal acquisition. In this work, we present a flexible 3 × 3 grid array sensor with a bioinspired support layer structure—derived from the Chinese Mi (米)-grid calligraphy framework. The support layer integration enables a 500-fold sensitivity enhancement over conventional unsupported designs, alongside an expanded sensing range, accelerated response time, improved signal resolution, and robust mechanical durability. When deployed for handwriting analysis, the sensor simultaneously captures trajectory, strength, and speed variations across its nine independent sensing units, enabling precise real-time monitoring. Integrated with an STM32 microcontroller and a convolutional neural network-based recognition algorithm, the system achieves exceeding 98% accuracy in handwriting identification while providing instant visual feedback via an LED display. Beyond its technical merits, the sensor's wearable design, multi-dimensional sensing capability, and real-time interactivity position it as a transformative solution for applications including smart writing interfaces, digital education tools, biometric authentication, and adaptive human–machine systems. The demonstrated capabilities establish a scalable pathway for advancing personalized wearable electronics and intelligent human–computer interaction technologies, with direct relevance to consumer and industrial applications.

Supplementary material for this article is available online

Keywords: strain sensor, nine-grid array, convolutional neural network, handwriting recognition

[5] These authors contributed equally to this work.
[*] Author to whom any correspondence should be addressed.

1. Introduction

Handwriting, a direct manifestation of human writing behavior, serves not only as a universal medium for information recording and communication but also as a critical interface for human–computer interaction (HCI). Traditional handwriting recognition systems, which rely on rule-based algorithms and labor-intensive feature extraction, face inherent limitations in efficiency and adaptability to individual writing styles [1–3]. Recent advances in flexible sensing technologies have transformed this field by enabling direct acquisition of handwriting kinematics (e.g. trajectory, pressure dynamics) through conformal sensor-device integration [4]. By coupling these sensors with neural networks, researchers now achieve unprecedented recognition accuracy while preserving the natural tactility of writing, thereby redefining interactive experiences [5–9]. These developments hold strategic implications for emerging applications ranging from biometric authentication to adaptive augmented reality interfaces [10, 11].

Current efforts to optimize flexible sensor-based recognition systems focus on two parallel strategies: (1) microstructural engineering of sensing materials to enhance electromechanical sensitivity and dynamic response, and (2) algorithmic optimization to decode complex spatiotemporal handwriting patterns. For instance, Sun *et al* [12] demonstrated a micro-pyramid-structured piezoresistive sensor capable of resolving sub-millimeter writing trajectories, while Ma *et al* [13] achieved multilingual text recognition using hydrogel-based strain sensors with self-adaptive interfacial adhesion. Ruan *et al* [14] created a three-dimensional (3D) force sensor capable of accurately decoupling 3D spatial force and attaching it to the fingertip to extract detailed handwriting information; Derrick Boateng [15] utilized a one-dimensional convolutional neural network (CNN) algorithm in conjunction with an ion-conducting flexible strain sensor based on dual-network hydrogel, achieving intelligent and accurate chirographic handwriting recognition with an accuracy rate of 96.3%. Despite these advances, critical challenges persist in simultaneously addressing sensitivity-speed-accuracy trade-offs and capturing writer-specific biometric features (e.g. gender-linked pressure profiles, velocity patterns) [16].

In this study, we developed a flexible 3 × 3 grid array sensor (GGAS) inspired by the structural principles of the traditional Chinese Mi (米) grid calligraphy training system. The sensor comprises three functional layers: (1) a copper interdigital electrode layer for high-fidelity signal transduction, (2) a laser-induced graphene (LIG)-patterned polyimide (PI) sensing layer (LIG/PI) optimized for strain-dependent resistive response, and (3) a 3M adhesive interlayer ensuring mechanical stability while minimizing hysteresis [17]. This hierarchical design enhances both sensitivity and response speed. By synchronously analyzing piezoresistive signals from the nine independent sensing channels and processing them via a hybrid neural network architecture, we achieved simultaneous recognition of writer-specific biometric features, including gender, writing strength characteristics, and writing trajectory (with an accuracy rate exceeding 98%). Furthermore, the integration of an embedded microcontroller-based monitoring system enables real-time visualization of handwriting kinematics, significantly improving the intuitiveness of HCI and demonstrating the sensor's potential for next-generation adaptive HCI platforms.

2. Experimental section

2.1. Preparation of precursor materials

A 50 μm-thick polyimide (PI) film (Guangzhou Beilong Electronics Co., Ltd) and a 0.15 mm-thick double-sided conductive copper foil (Shenzhen Wangxing Tape Co., Ltd) were selected as precursor materials. The PI film was cleaned three times on both sides with anhydrous ethanol and then dried in an oven at 80 °C for 30 min to remove surface contaminants. The film was subsequently laser-cut into 3.4 cm × 3.4 cm substrates. For electrode fabrication, a copper foil was uniformly adhered onto a piece of PI film, forming a PI/Cu composite substrate.

2.2. Preparation of the sensing layer

A UV laser cutting system (CY-ZW3W, Shenzhen Chaoyue Laser) was employed to induce the formation of LIG on the surface of the PI film. Optimized laser parameters were set as follows: pulse frequency of 180 kHz, pulse width of 5 μs, and scanning speed of 20 mm s^{-1}, with single-pass processing. A 3 × 3 array of LIG sensing units was patterned, with each unit measuring 1 cm × 1 cm and a spacing of 0.2 cm between adjacent units, resulting in a regular grid layout.

2.3. Preparation of the electrode layer

The PI/Cu composite substrate was patterned into a 3 × 3 interdigitated electrode array using high-frequency laser ablation. The laser parameters were: pulse frequency of 50 kHz, pulse width of 2 μs, scanning speed of 800 mm s^{-1}, and 80 passes. After patterning, conductive silver paste (solid content: 68%, Senglue Technology) was applied to the electrode leads to bond external copper wires for electrical connection.

2.4. Preparation of support layer

To enhance the mechanical stability and alignment accuracy between the sensing and electrode layers, a support layer was introduced. A 3.4 cm × 3.4 cm piece of 3M adhesive tape (thickness: 110 μm) was laser-cut into a 3 × 3 grid frame using the same parameters as for the electrode layer. The support frame was laminated around the edges of the LIG sensing units, maintaining flexibility while providing structural support.

2.5. Sensor assembly

The sensing layer (integrated with the support layer) and the electrode layer were laminated face-to-face, ensuring precise

alignment between the LIG sensing units and the corresponding interdigitated electrodes.

The fabrication of the GGAS without the support layer omitted the 2.4 step (preparation of support layer), while the remaining steps remained consistent with the above procedure.

3. Results and discussion

The preparation process for the GGAS is shown in figure 1(a). The sensor is prepared using laser-induced graphitization and laser-cutting techniques to define the LIG/PI sensing layer, copper interdigitated electrodes, and 3M adhesive support layer [18]. Figure 1(b) shows the sensor conformally worn on the back of a human hand, demonstrating its flexibility, skin adherence, and wearability under natural conditions. An enlarged view of the sensor array, marked in figure 1(b) and shown in detail in figure 1(c), reveals the compact 3 × 3 layout of sensing units on a 34 mm × 34 mm PI substrate. This design enables each unit to independently respond to mechanical stimuli, supporting high-resolution spatial sensing. The performance of the LIG sensing layer is critical to the overall sensor performance. Therefore, we investigated the effects of two key parameters—laser scanning frequency (170, 180, 190 kHz) and scanning speed (10, 20, 30 mm s^{-1})—on LIG formation. Optical images of the nine sample groups are presented in figure S1, showing that conductivity increased with higher scanning frequencies and speeds [19] (table S1). SEM characterization (figure S2) reveals that the LIG exhibits ordered graphene stripes [20], with the surface at 180 kHz and 20 mm s^{-1} displaying a dense, porous layered structure (figure 1(d)). Raman spectroscopy (figures S3(a)–(c)) confirms the presence of three characteristic peaks of graphene: *D* peak at 1350 cm^{-1}, *G* peak at 1580 cm^{-1}, and 2*D* peak at 2670 cm^{-1} [21, 22]. Notably, the absence of clear 2*D* peaks in samples scanned at 190 kHz indicates poorer electrical conductivity (figure S3(c)). The lower intensity ratios (I_D/I_G) observed at 180 kHz and 170 kHz with scanning speeds of 10 and 20 mm s^{-1} in figure S3(d) suggest that graphene has fewer defects and a high conversion rate [23, 24], indicating that most carbon atoms are arranged in an ideal graphene structure [25]. Furthermore, as shown in figure S3(e), the I_{2D}/I_G ratio reaches its highest value at 180 kHz and 20 mm s^{-1}, which signifies superior electrical conductivity (figure 1(e)) [24]. Taking into account both processing efficiency and graphene quality, the parameters of 180 kHz and 20 mm s^{-1} are selected as the optimal conditions for LIG generation.

Comprehensive force–electricity testing of the flexible strain sensor unit is crucial for evaluating its performance. Figure 2(a) illustrates the schematic structure of the LIG/PI flexible strain sensor and the electrical signal changes when pressure is applied to the sensor. Without the 3M adhesive support layer, the graphene and copper interdigitated electrodes of sensor only make surface contact. As pressure increases, the contact area deforms, compressing the graphene structure and enhancing the conductive pathways, leading to a decrease in

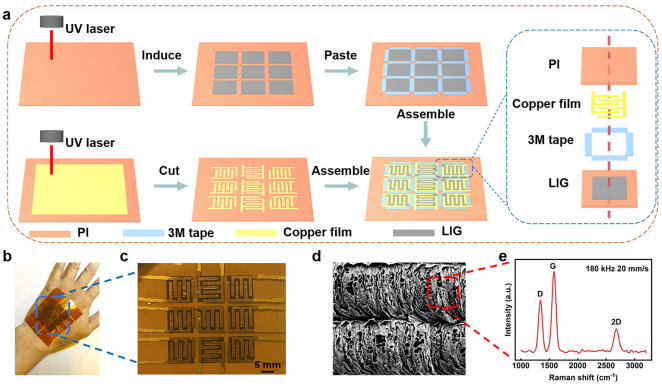

Figure 1. (a) Schematic flow diagram of the preparation process of the GGAS. (b) Optical diagram of the GGAS worn on the back of the hand. (c) Optical diagram of the assembled GGAS. (d) Scanning electron microscopy characterization of LIG. (e) Raman pattern of LIG on PI.

resistance [20]. Test results from a universal mechanical testing machine confirm the sensing mechanism. When a load ranging from 0 to 25 N is applied, the sensor's resistance gradually decreases with a sensitivity of −0.000 80 kPa^{-1}. However, further increases in load causes the sensitivity to diminish (figure 2(b)). In contrast, when the LIG/PI flexible strain sensor unit is equipped with a support layer, its sensitivity improves, allowing it to measure in a wider range of pressures (0–60 N). As pressure increases, both the displacement and resistance of the sensor change accordingly (figure S4). The addition of the support layer alters the sensor's behavior. When no pressure is applied, there is no contact between the graphene and the copper interdigitated electrodes, resulting in an open circuit with infinite resistance, which reduces circuit losses compared to the unsupported configuration. When pressure is applied, the sensor undergoes three distinct stages (figure 2(d)): Stage 1: As pressure increases from 0 to 20 kPa, the contact area between the graphene and electrodes expands, leading to a decrease in resistance from an initially infinite value (disconnected state) to a measurable level. The sensor exhibits its highest sensitivity of −0.032 kPa^{-1} during this stage (figure 2(e)); Stage 2: As pressure continues to increase from 20 to 200 kPa, near-complete contact is established between the electrodes and the LIG/PI layer. Further compression of the graphene's microstructure becomes the dominant factor influencing resistance changes, resulting in a gradual decrease in sensitivity; Stage 3: When the pressure exceeds 200 kPa, the sensor's resistance stabilizes and sensitivity approaches zero. At this point, the LIG/PI material has reached its maximum compression limit, preventing any further significant deformation [26, 27]. Comparing the performance of the sensors with and without the support layer (figures 2(c) and (f)), the response time decreases from 277 ms to 157 ms, while the recovery time reduces from 543 ms to 184 ms. The substantial improvement in both response and recovery times enhances the sensor's

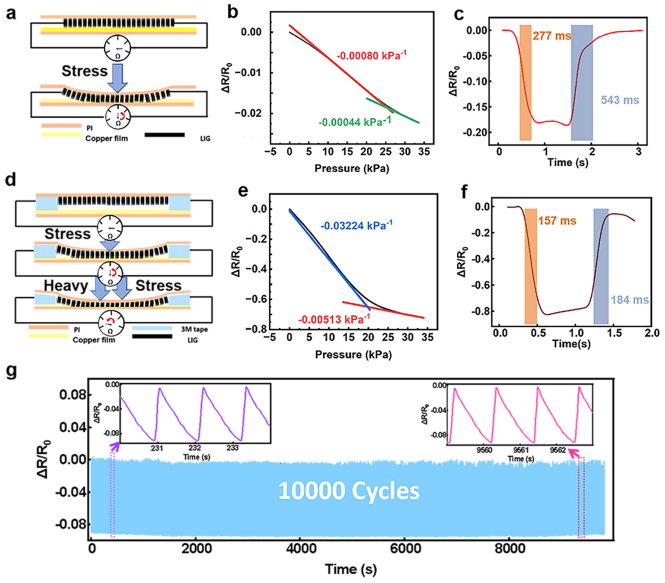

Figure 2. Sensing mechanism (a), sensitivity (b) and response time (c) of the GGAS without support layer. Sensing mechanism (d), sensitivity (e), response time (f) and long-cyclic loading test of the GGAS with a support layer.

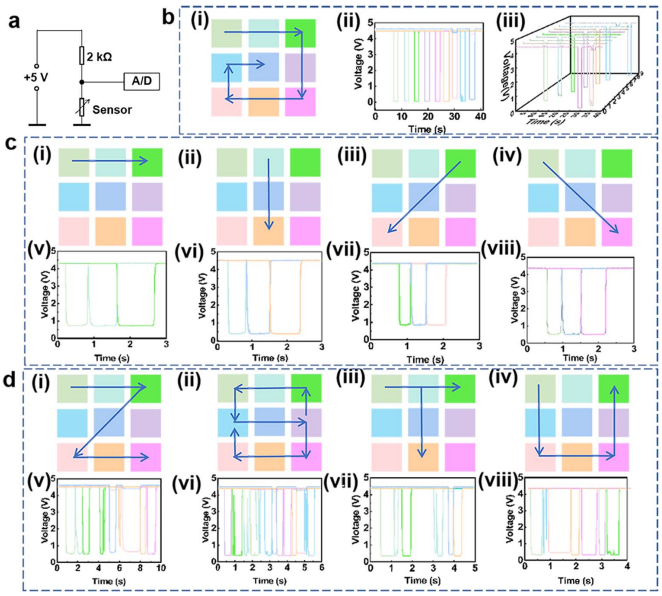

Figure 3. (a) Logic diagram of voltage divider circuit. (b) Writing trajectory of the sensor (i), corresponding nine-channel electrical signal changes (ii) and waterfall diagram (iii). (c) Schematic diagram of writing strokes of 'horizontal,' 'vertical,' 'left-falling,' and 'right-falling' in sequence (i–iv) and corresponding nine-channel electrical signal changes (v–viii). (d) Schematic diagram of writing letters of 'Z', 'S', 'T', and 'U' in sequence (i–iv) and corresponding nine-channel electrical signal changes (v–viii).

potential for real-time monitoring and rapid-response applications. Additionally, the sensor demonstrates stable electrical signal output during approximately 10 000 long-cycle loading tests (figure 2(g)), conducted using the MX-0350 mechanical testing system (Jiangsu Moxin Industrial Systems Co., Ltd, China) under a consistent applied force of 15 N (sampling rate: 10 Hz; loading frequency: 1 Hz). These results convincingly demonstrate the sensor's excellent reliability and mechanical durability, underscoring its suitability for long-term practical applications [28].

As a functional demonstration, GGAS was used as a handwriting tablet implementation. For this purpose, we constructed a signal acquisition system based on the 3 × 3 grid sensor array. The system comprises a voltage divider circuit and a multiplexed signal acquisition card. The circuit is powered by the computer's USB port (approximately 5 V), and the voltage divider resistance is carefully selected based on the resistance change characteristics of the sensor. The voltage divider circuit quantifies the strain on the sensor by measuring resistance changes in the sensing units under the pressure of handwriting (figure 3(a)). The multiplexed signal acquisition card converts the analog signals from the voltage divider into digital signals for further processing. To distinguish between different sensing units, each unit in the 3 × 3 array was assigned a unique identifier using distinct colors and numbers, as shown in figure S5. When writing followed the sequence depicted in figure 3 b(i), the corresponding electrical signals from the nine sensing units were recorded sequentially, precisely matching the writing trajectory (figures 3(b-ii) and (b-iii)). The sensor's ability to accurately capture the independent changes of each sensing unit ensures reliable data for handwriting trajectory recognition and parsing. This capability highlights the potential of the GGAS in applications requiring precise and high-resolution signal detection.

The legibility of electrical signals during continuous writing is crucial for accurately capturing handwriting trajectories. To evaluate this capability, we tested the writing of basic strokes including 'horizontal,' 'vertical,' 'left-falling,' and 'right-falling' (figure 3(c)). For the horizontal stroke, figures 3(c-i) and (c-v) illustrate that the sensing units 1, 2, and 3 in the sensor array produce significant electrical signal changes. These changes strictly follow the order of the writing sequence, with no interference between adjacent sensing units. Similarly, the sensor accurately captures the writing trajectories of other basic strokes, as demonstrated in figures 3(c-ii)–(c-viii). Beyond recording trajectories, the sensor also enables the inference of finger movement speed across different sensing units by analyzing the temporal variations in the electrical signals. Additionally, figure 3(d) illustrates the electrical signal changes during the writing of the abbreviation 'Z S T U' for Zhejiang Science and Technology University. The experimental results clearly depict the process and trajectory of writing each letter. Taking the letter 'U' as an example, figure 3(d-viii) displays electrical signal changes corresponding to the finger passing through the seven sensing units: 1, 4, 7, 8, 9, 6 and 3 in sequence figure 3(d-iv)). These transitions generate seven distinct falling edges in the electrical signal, reflecting the trajectory of writing 'U' with high precision. This ability to convert electrical signals into written content demonstrates the high accuracy and reliability of the GGAS for capturing handwriting trajectories. The results further highlight

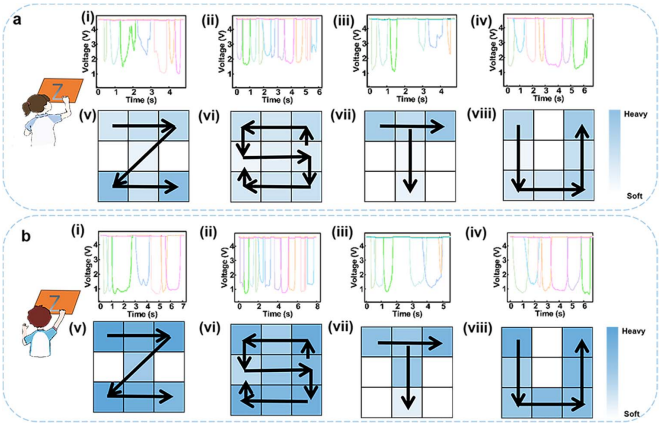

Figure 4. (a) Electrical signals changes of female volunteers writing 'Z', 'S', 'T', and 'U' (i–iv) and the corresponding intensity depth maps (v–viii). (b) Electrical signals changes of male volunteers writing 'Z', 'S', 'T', and 'U' (i–iv) and the corresponding intensity depth maps (v–viii).

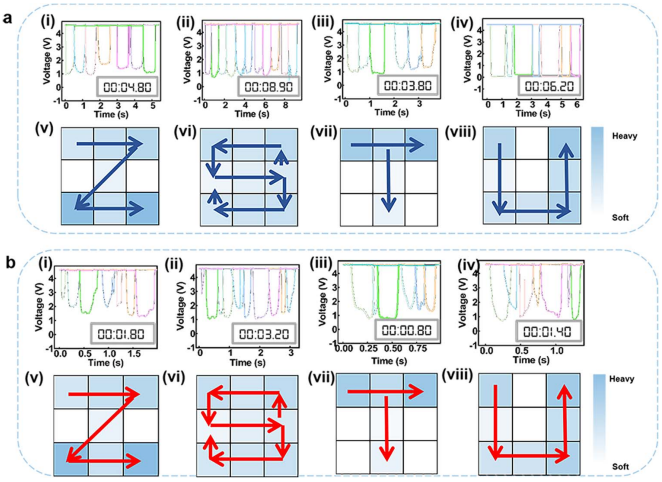

Figure 5. Plot of electrical signal changes and corresponding force depths of the GGAS at different writing speeds, with inset showing writing time.

the sensor's potential for use in handwriting recognition and related applications.

To further distinguish the differences in handwriting strength, we conducted handwriting recognition experiments involving male and female volunteers. During the experiments, participants wrote the abbreviation 'Z S T U,' and the collected electrical signals exhibited noticeable differences (figure 4). The female volunteers apply less pressure while writing, resulting in relatively weak changes in the electrical signals. Conversely, the male volunteers exert greater force, leading to more pronounced signal fluctuations. By analyzing the sequence of signal peaks, the written content could be accurately identified. Additionally, depth maps visualizing peak signal variations intuitively highlight the differences in pressure applied during the writing process between male and female volunteers.

Furthermore, the handwriting board based on the GGAS effectively demonstrates its capability to analyze the user's writing speed. Figure 5 compares electrical signals recorded from the same volunteer writing the same letters with different speeds. The inset provides a detailed view of the writing duration, which was calculated based on the temporal changes in the electrical signals. Depth maps of the peak electrical signals accurately characterize both the writing trajectory and applied force. A comparison of figures 5(a) and (b) reveals that faster writing results in lower signal peaks, likely due to reduced pressure applied to the sensor during higher writing speeds. This versatile and personalized capability to recognize trajectory, strength and speed makes the GGAS an ideal solution for advanced handwriting recognition applications.

To provide users with a more intuitive perception of writing trajectories and characteristics, we developed a handwriting recognition system based on the GGAS (figure 6(a)). The system utilizes an STM32 microcontroller as the central control unit (figure S6), capturing real-time voltage signals from the sensor's nine channels via its ADC module [29]. Then, a CNN is employed for deep learning and signal processing to enhance the accuracy and efficiency of handwriting recognition [30, 31]. As illustrated in figure 6(b), the network accepts a 3×3 sensor-grid input (9 nodes) and propagates it through two fully connected hidden layers of 128 and 64 ReLU-activated units, respectively, with hierarchical dropout rates of 30% and 20% to mitigate overfitting. A 36-way Softmax layer produces the final classification. Training was performed on a dataset of 100 000 labeled samples—partitioned 70%/10%/20% into training, validation, and test subsets—using the Adam optimizer (initial learning rate 1×10^{-3} with scheduled decay). The model converged after 75 epochs (100 mini-batch iterations per epoch), achieving a stabilized cross-entropy loss of 0.1, which reflects an optimal balance between feature learning and regularization [32]. Post-training MATLAB analyses revealed well-defined handwriting trajectories, pressure distributions, and temporal dynamics. In a validation study with 12 participants each writing the character 'A,' CNN-enabled system achieved a recognition accuracy exceeding 98%, as confirmed by the confusion matrix in figure 6(c) [33]. To enhance wearability and real-time interactivity, the microcontroller was integrated with an external LED display (figure 6(d)), enabling immediate visualization of handwritten input. Compared with previously reported handwriting recognition sensors (table S2) [12, 34–38], our sensor stands out for its high recognition accuracy (>98%) and well-balanced overall performance, with a sensitivity of $-0.032\ \mathrm{kPa}^{-1}$ and a response time of 157 ms. Beyond stable signal response characteristics, it uniquely supports multi-dimensional sensing functions—including detection of

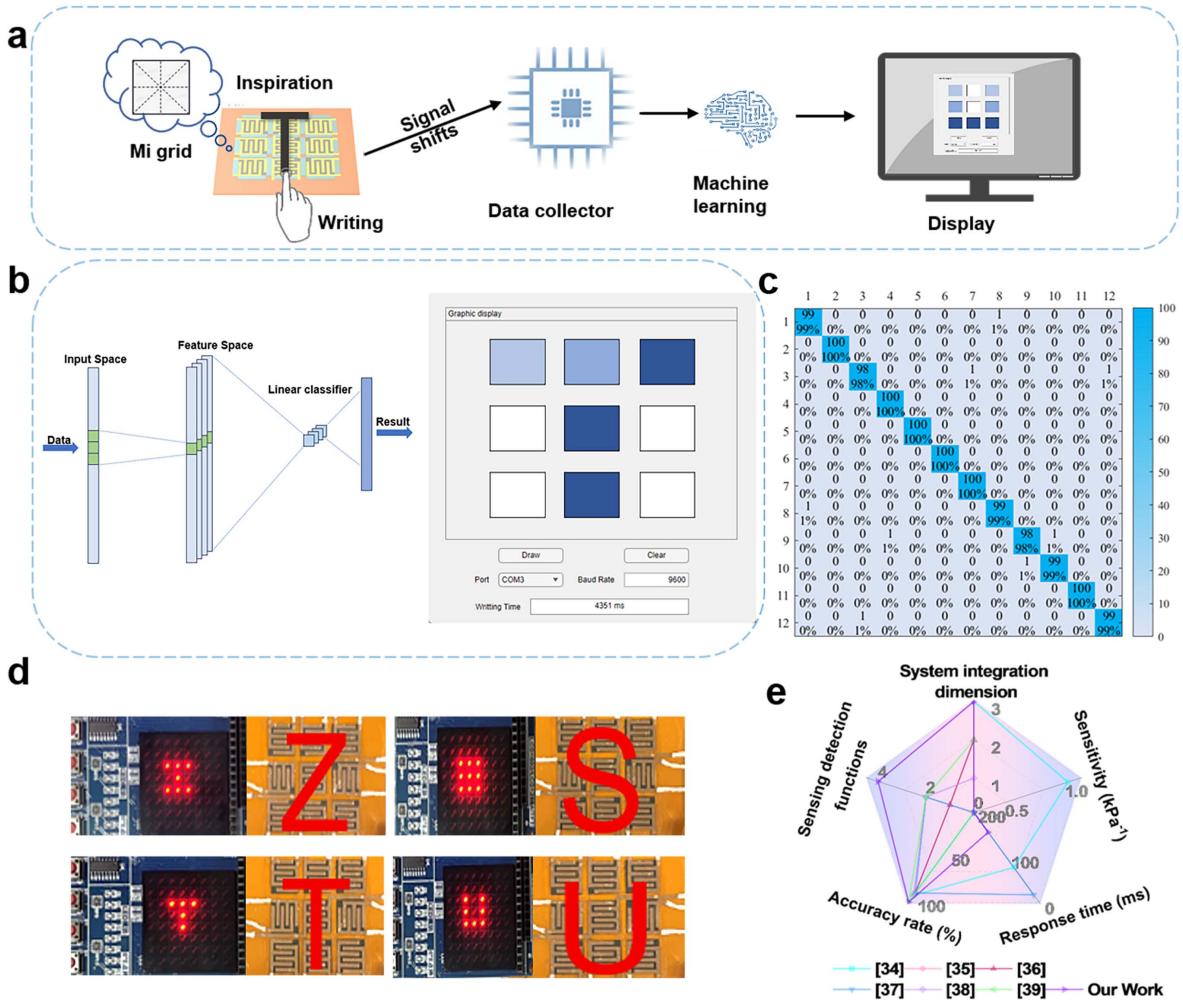

Figure 6. (a) Workflow diagram of handwriting recognition system based on the GGAS. (b) Schematic diagram of convolutional neural network. (c) Accuracy of writing letter 'A' by 12 volunteers. (d) Optical diagram of the microcontroller external display for handwriting recognition display. (e) Radar chart comparing the performance of this work with previously reported handwriting recognition strain sensors.

writing trajectory, strength, speed, and user characteristics—alongside integrated features such as real-time visualization, continuous monitoring, and a wearable form factor. These comparative advantages are visually summarized in a radar chart (figure 6(e)), derived from the key data in table S2, further highlighting the system's strengths and its strong potential for practical applications in handwriting recognition and wearable electronics [39].

4. Conclusions

In conclusion, we have developed a flexible GGAS incorporating a support layer structure that enables accurate handwriting recognition and trajectory capture. The introduction of the support layer dramatically enhances sensor performance, achieving a 500-fold increase in sensitivity compared to the unsupported design, along with an extended sensing range, accelerated response time, improved signal resolution, and outstanding mechanical durability. The integrated data acquisition system effectively captures subtle signal variations across multiple sensing units, facilitating precise, real-time monitoring of handwriting trajectory, pressure, and speed. By integrating an STM32 microcontroller and applying CNN-based pattern recognition technology, the system's handwriting recognition accuracy exceeds 98%, and an external LED display provides instant visualization of the input, enhancing the potential for real-time interaction. Beyond its technical strengths, the sensor's combination of high recognition accuracy, multi-dimensional sensing functionality, real-time responsiveness, and wearable design renders it highly suitable for applications such as smart writing systems, digital education platforms, secure user authentication, and next-generation wearable electronics. Moreover, its ability to capture user-specific handwriting characteristics unlocks new possibilities in biometric profiling and advanced human–machine interfaces. Collectively, these advantages highlight the sensor's substantial potential for commercialization and broader deployment in both consumer and industrial domains.

Data availability statement

All data that support the findings of this study are included within the article (and any supplementary files).

Acknowledgments

This work was supported by the National Natural Science Foundation of China (Nos. 12272351, 62401509 and 12372168), the Youth Top-notch Talent Project of Zhejiang Ten Thousand Plan of China (No. ZJWR0308010), the Zhejiang Provincial Natural Science Foundation of China (Nos. LZ24A020004 and LRG25A020001), the 'Pioneer' and 'Leading Goose' R&D Program of Zhejiang (Grant No. 2023C01051).

ORCID iDs

Ziyi Pei https://orcid.org/0009-0007-1937-2030
Aiping Liu https://orcid.org/0000-0002-2338-062X

References

[1] Tariq M U and Aqab S 2020 Handwriting recognition using artificial intelligence neural network and image processing *Int. J. Adv. Comput. Sci. Appl.* **11** 710–9
[2] Senthil T, Rajan C and Deepika J 2022 An efficient handwritten digit recognition based on convolutional neural networks with orthogonal learning strategies *Int. J. Pattern Recognit. Artif. Intell.* **36** 2253001
[3] Salkanovic A, Bačnar D, Sušanj D and Ljubic S 2024 A sensor-fusion-based experimental apparatus for collecting touchscreen handwriting biometric features *Appl. Sci.* **14** 11234
[4] Qin X K, Zhong B W, Xu H, Jackman J A, Xu K C, Cho N J, Lou Z and Wang L L 2025 Manufacturing high-performance flexible sensors via advanced patterning techniques *Int. J. Extreme Manuf.* **7** 032003
[5] Li Z, Xu H, Zheng Y, Liu L, Li L, Lou Z and Wang L 2025 A reconfigurable heterostructure transistor array for monocular 3D parallax reconstruction *Nat. Electron.* **8** 46–55
[6] Li L, Xu H, Li Z, Zhong B, Lou Z and Wang L 2025 3D heterogeneous sensing system for multimode parrallel signal no-spatiotemporal misalignment recognition *Adv. Mater.* **37** 2414054
[7] Jiang L, Liu J, He S, Liu A, Zhang J, Xu H and Shao W 2022 Flexible wearable sensors based on lignin doped organohydrogels with multi-functionalities *Chem. Eng. J.* **430** 132653
[8] Cai Z, Li Y, Fan P, Hu Q and Zhu Z 2023 High-sensitivity gradient porous ionic polymer pressure sensor in charge-sensing mode *Appl. Phys. Lett.* **122** 7
[9] Xu W, Ren Q, Li J, Xu J, Bai G, Zhu C and Li W 2024 Triboelectric contact localization electronics: a systematic review *Sensors* **24** 17
[10] Yang C Q, Zhang D, Wang D, Luan H, Chen X and Yan W 2023 In situ polymerized MXene/polypyrrole/hydr-oxyethyl cellulose-based flexible strain sensor enabled by machine learning for handwriting recognition *ACS Appl. Mater. Interfaces* **15** 5811–21
[11] Miao G, Liu Q, Shi Y, Ci R, Liu G and Shan F 2024 Artificial synapses based on boron ions-modulated transistors for neuromorphic applications *Appl. Phys. Lett.* **124** 203301
[12] Sun F Q *et al* 2019 Novel flexible pressure sensor combining with dynamic-time-warping algorithm for handwriting identification *Sens. Actuators A* **293** 70–76
[13] Ma Y H, Zhang D Z, Wang Z H, Zhang H, Xia H, Mao R Y, Cai H L and Luan H X 2023 Self-adhesive, anti-freezing MXene-based hydrogel strain sensor for motion monitoring and handwriting recognition with deep learning *ACS Appl. Mater. Interfaces* **15** 29413–24
[14] Ruan D Q, Chen G, Luo X, Cheng L, Wu H and Liu A 2024 Bionic octopus-like flexible three-dimensional force sensor for meticulous handwriting recognition in human-computer interactions *ACS Nano Energy* **123** 109357
[15] Du B, Yin M, Yang K, Wang S, Pei Y, Luo R, Zhou S and Li H 2024 Ultrafast polymerization of a self-adhesive and strain sensitive hydrogel-based flexible sensor for human motion monitoring and handwriting recognition *Polymers* **16** 1595
[16] Nagaraju M 2022 Digital handwriting recognition using hand tracking with MediaPipe and OpenCV libraries *Int. J. Res. Appl. Sci. Eng. Technol.* **10** 659–66
[17] Yu T, Tao Y, Wu Y, Zhang D, Yang J and Ge G 2023 Heterogeneous multi-material flexible piezoresistive sensor with high sensitivity and wide measurement range *Micromachines* **14** 716
[18] Han Y R, Han Y K, He Q H, Liu H, Zhang Y and Han L 2023 Ultrasensitive and reliable SERS chip based on facile assembly of AgNPs on porous LIG to enhance the local electromagnetic field *J. Phys. Chem. C* **127** 4195–202
[19] Cheng L *et al* 2023 Laser-induced graphene strain sensor for conformable lip-reading recognition and human-machine interaction *ACS Appl. Nano Mater.* **6** 7290–8
[20] Hao D, Yang R, Yi N and Cheng H 2021 Highly sensitive piezoresistive pressure sensors based on laser-induced graphene with molybdenum disulfide nanoparticles *Sci. China Technol. Sci.* **64** 2408–14
[21] Yoon D, Moon H, Cheong H, Choi J, Choi J and Park B 2009 Variations in the Raman spectrum as a function of the number of graphene layers *J. Korean Phys. Soc.* **55** 1299
[22] Qian Y, Pei C, Ke H, Wei X, Wang D, Jia Y, Sun B, Wang G and Wang W 2025 Ultra-stable Co-based metallic glassy microwires for highly sensitive giant-magnetoimpedance sensors *Sci. China Phys. Mech. Astron.* **68** 24611
[23] De la Roche J, López—Cifuentes I and Jaramillo—Botero A 2023 Influence of lasing parameters on the morphology and electrical resistance of polyimide—based laser—induced graphene (LIG) *Carbon Lett.* **33** 587–95
[24] Zhao Y, Wang S, Wang X, Zhang L, Sha J, Zhang X, Mu R, Dong Z 2024 Coal-based graphene formation by CO_2 laser scribing: various structures and excellent electrochemical performance *Fuel* **373** 132318.0016–2361
[25] Xu J *et al* 2024 Effect of phase separation size on the properties of self-healing elastomer *Chin. J. Polym. Sci.* **42** 798–804
[26] Liu Y, Chen L, Yang Y, Chen H, Zhang X and Liu S 2022 High mechanical strength and multifunctional microphase-separated supramolecular hydrogels fabricated by liquid-crystalline block copolymer *Macromol. Rapid Commun.* **44** 2200829
[27] Chen Y C, Zhang P, Li Y, Zhang K, Su J and Huang L 2021 Flexible capacitive pressure sensor based on multi—walled carbon nanotubes microstructure electrodes *J. Appl. Phys.* **54** 155101
[28] Zhao Y *et al* 2021 Graphene/SnS_2 van der Waals photodetector with high photoresponsivity and high photodetectivity for broadband 365–2240 nm detection *ACS Appl. Mater. Interfaces* **13** 47198–207
[29] Wang T, Wang C, Zeng Q, Gu G, Wang X, Cheng G and Du Z 2024 A real-time, self-powered wireless pressure sensing

system with efficient coupling energy harvester, sensing, and communication modules *Nano Energy* **125** 109533
[30] Lu Y, Kong D, Yang G, Wang R, Pang G, Luo H, Yang H and Xu K 2023 Machine learning-enabled tactile sensor design for dynamic touch decoding *Adv. Sci.* **10** 2303949
[31] Biswas A and Islam M S 2023 A hybrid deep CNN-SVM approach for brain tumor classification *J. Inf. Syst. Eng. Bus. Intell.* **9** 1–15
[32] Li G Q and Yang X 2023 The training gesture recognition and early warning method based on CNN model *Wirel. Pers. Commun.* (https://doi.org/10.1007/s11277-023-10471-8)
[33] Ahmad S, Ansari S U, Haider U, Javed K, Rahman J U and Anwar S 2022 Confusion matrix-based modularity induction into pretrained *CNN. Multimed. Tools Appl.* **81** 23311–37
[34] Zhang P, Wang X, Li Y, Zhang K and Huang L 2023 Plantar pressure monitoring system based on a flexible pressure sensor array for human walking feature recognition *IEEE Trans. Electron Devices* **70** 6526–33
[35] Lou C, Wang S, Liang T, Pang C, Huang L, Run M and Liu X 2017 A graphene-based flexible pressure sensor with applications to plantar pressure measurement and gait analysis *Materials* **10** 1068
[36] Kristanto H, Sathe P, Schmitz A, Tomo T P, Somlor S and Sugano S 2018 A wearable three-axis tactile sensor for human fingertips *IEEE Robot. Autom. Lett.* **3** 4313–20
[37] Guo Z, Xiao F, Sheng B, Fei H and Yu S 2020 WiReader: adaptive air handwriting recognition based on commercial WiFi signal *IEEE Int. Things J.* **7** 10483–94
[38] Ott F, Rügamer D, Heublein L, Hamann T, Barth J, Bischl B and Mutschler C 2022 Benchmarking online sequence—to—sequence and character—based handwriting recognition from IMU—enhanced pens *Int. J. Doc. Anal. Recogn.* **25** 385–414
[39] Xu K C, Cai Z M, Luo H Y, Lu Y Y, Ding C L, Yang G, Wang L L, Kuang C F, Liu J Q and Yang H Y 2024 Towards integrated multifunctional laser-induced graphene-based skin-like flexible sensor systems *ACS Nano* **18** 26435–76